On the Transmitted Beam Degradation through FSS in the Working Band by Plane-wave Spectrum Computation and Evaluation

Ming Jin [1,2] and Ming Bai [2†]

[1] State Key Laboratory of Remote Sensing Science
Institute of Remote Sensing and Digital Earth Chinese Academy of Sciences (CAS), Beijing, 100101, China P. R.
Jinmingaps@163.com

[2] School of Electronic Information Engineering
BEIHANG University, Beijing, 100191, China P. R.
[†]mbai@buaa.edu.cn

Abstract ─ In this paper, we implemented the combination of FDTD (Finite Difference Time Domain) and the plane-wave spectrum (PWS) algorithms, to evaluate beam transmission through frequency selective surface (FSS) in the near field region. The hybrid method takes advantage of the FDTD for the wideband analysis ability, and that of the PWS theory in the rapid re-composition for transmitted fields due to variable beam incidence. Consequently, it meets the need of beam transmission evaluation in the working band when the FSS is located among a serial of components, as in a millimeter Quasi-Optical (QO) instrument. After verifying the hybrid approach by results of other methods, we studied the degradations in the transmitted beams through an FSS design within the band of interest. The investigations are performed at the view of the transmission coefficient distributions in the PWS. It is found that the transmitted beam distortion is due to the non-flatness of the transmission coefficient distribution in the spectrum region covered by the beam incidence.

Index Terms ─ Beam transmission, frequency selective surfaces, plane-wave spectrum, quasi optical instruments.

I. INTRODUCTION

The frequency selective surface (FSS) has been widely employed as the beam filter in microwave and optical applications. Being artificial periodic structures, reflection and transmission properties of an FSS can be efficiently calculated by modeling only one single unit under the periodic boundary condition (PBC) [1-5], due to plane-wave incidence. In case a size-limited beam other than a plane wave needs to be evaluated, which is more realistic, the analysis on transformation of the beam by an FSS can be more challenging. Techniques and methods have been developed [6-7], strengthened by the plane-wave spectrum (PWS) concept, treating arbitrary beam as a combination of plane waves from different directions. In our previous works, the transmitted fields through an FSS [8] and scattering from a periodic cone structure [9] under variable beam incidence were computed by the FDTD-PWS hybrid approach. It was highlighted that the calculated field responses to each plane-wave (by PBC simulations) can be reused, for further evaluations on the fields due to any varied beam incidence, which can be instantly obtained by simply recomposing the pre-calculated responses [9]. However, the PBC condition used in those works is functional only at a single frequency, as a result the advantage in the wideband analysis ability of FDTD algorithm wasn't token.

In practical applications, such as in the millimeter quasi-optical (QO) feed instruments for reflector antennas as in Fig. 1, it is necessary to design a serial of components to construct the beam path, where the near fields of transmitted beam through an FSS should be evaluated accurately [10-15]. Also, it is significant to meet the need of analyzing the changing patterns of beam transmission through FSS via variable beam incidence (etc., with different beam waist radius), which is cared by QO designers in the design and optimization process [11-15]. And in practice, one would like to know the frequency response in a band other than at a point. Motivated by this need and the wideband FDTD-PBC technique reported in [3], we are to update and complete the FDTD-PWS hybrid method for modeling planar periodic structures under beam illuminations.

Similar works on the hybrid of FDTD and PWS should be mentioned [16-17]. In those reports, results by PBC simulations are used to compose the fields in periodic structures due to a current source illumination. Such a hybrid is convenient for wideband investigations, because both the PBC simulations and field composition are performed in the time domain. However, for evaluating beam transmission through FSS, pre-calculated field responses to each plane-wave cannot be re-used in

Submitted On: July 26, 2014
Accepted On: June 17, 2016

the time domain re-composition, for fields due to a varied beam incidence. This is because the waveform (in time) of each equivalent current source (for presenting the beam) changes as the beam incidence varies, while in that scheme the same waveform is shared by the illuminating current and excitation signals in PBC simulations. On the contrary, we chose to conduct the field composition in frequency domain, while the time-domain PBC simulations offer necessary results within the frequency band of interest, as in Fig. 2. In this way, the proposed FDTD-PWS combination can handle beam transmission evaluation through FSS in the pass band, while the PBC simulation results can be re-used for variable beam incidence. It should be stated that the two hybrid approaches of FDTD and PWS share the same spirit in principle, but are different in methodology as aimed at different applications.

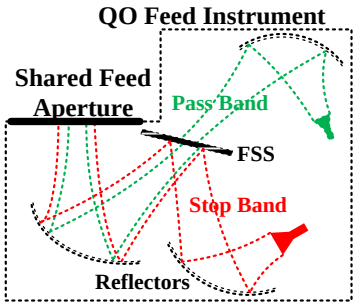

Fig. 1. Sketch of a FSS structure in a QO feed instrument.

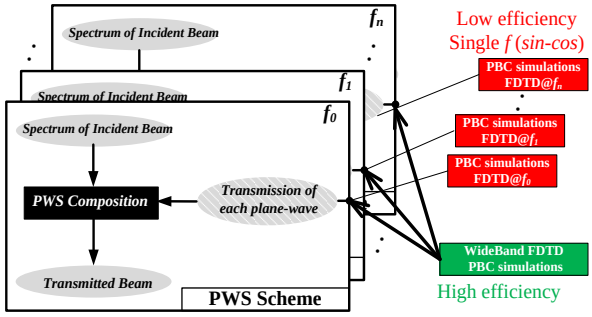

Fig. 2. Diagram of the band FDTD-PWS hybrid for analyzing beam transmission through FSS in the pass band.

For validating the updated FDTD-PWS hybrid method, we use the results obtained by directly modeling a finite-sized FSS screen with standard FDTD formulations. After that, we study the deforming effects on the transmitted beams by an FSS design within the pass band. The investigations are performed at the view of the transmission coefficient distributions in the PWS. As will be shown, such a spectrum analysis manner provides an intuitive perspective for beam propagation diagnostic through FSS.

The rest of this paper consists of five parts: in Section II, the configuration of beam transmission through FSS and the FDTD-PWS hybrid method is demonstrated; in Section III the FDTD-PWS calculations are verified; then the computation efficiency of the proposed hybrid is discussed in Section IV; in Section IV we study and discuss the deforming effects by the FSS; finally conclusions are drawn in Section V.

II. SECTION FORMATTING

A. Configuration

The configuration of beam transmission through FSS is presented in Fig. 3. Tangential components of the incident fields are sampled on the incident aperture (**IA**), for calculating the transmitted fields on the transmitted aperture (**TA**). And, the beam transmission coefficient T_b is defined as:

$$T_b = \frac{\iint (\vec{E}^t(x,y)|_{TA} \times \vec{H}^{t*}(x,y)|_{TA}) \cdot \hat{z} dxdy}{\iint (\vec{E}^i(x,y)|_{IA} \times \vec{H}^{i*}(x,y)|_{IA}) \cdot \hat{z} dxdy}. \quad (1)$$

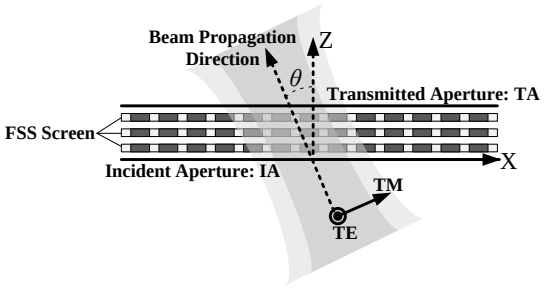

Fig. 3. Sketch of beam transmission through an FSS screen.

B. PWS solution for beam transmission through FSS

According to the PWS theory, tangential components of the transmitted fields at frequency f (wavelength λ) on **TA** can be obtained by using:

$$\begin{pmatrix} E_x^t(x,y)|_{TA} \\ E_y^t(x,y)|_{TA} \end{pmatrix} = \iint_{\left(k_x^2+k_y^2<k_0^2\right)} \tilde{M}(k_x,k_y,x,y) \begin{pmatrix} A_x^i(k_x,k_y) \\ A_y^i(k_x,k_y) \end{pmatrix} \frac{dk_x dk_y}{4\pi^2}, \quad (2)$$

where $k_0 = 2\pi/\lambda$, $k_x = k_0 sin\theta cos\varphi$, $k_y = k_0 sin\theta sin\varphi$; and $A^i_x(k_x,k_y)$ along with $A^i_y(k_x,k_y)$ stand for the PWS distributions of the incident fields $E^i_x(x,y)|_{IA}$ and $E^i_y(x,y)|_{IA}$ on **IA,** respectively. And,

$$\tilde{M}(k_x,k_y,x,y) = \begin{pmatrix} f^t_{xx}(k_x,k_y,x,y) & f^t_{xy}(k_x,k_y,x,y) \\ f^t_{yx}(k_x,k_y,x,y) & f^t_{yy}(k_x,k_y,x,y) \end{pmatrix}. \quad (3)$$

Here, $f^t_{\gamma\xi}(k_x,k_y,x,y)$ stands for the γ component distribution of the transmitted E-fields on **TA**, due to the plane-wave incidence of (k_x,k_y) with a unit ξ E-field component but without the other component. Here and in the rest of this paper, ξ and γ stand for x or y. The

$f^t_{\gamma\xi}(k_x,k_y,x,y)$ can be found from the results by PBC simulations of a single FSS unit, in which only the tangential ξ component of the incident E-field is included in the excitation via a soft source in FDTD.

Meanwhile, the incident spectrum $A^i_x(k_x,k_y)$ and $A^i_y(k_x,k_y)$ can be obtained by performing the inverse Fourier transform:

$$\begin{pmatrix} A^i_x(k_x,k_y) \\ A^i_y(k_x,k_y) \end{pmatrix} = \iint \begin{pmatrix} E^i_x(x,y)|_{IA} \\ E^i_y(x,y)|_{IA} \end{pmatrix} \cdot \mathrm{e}^{j(k_x\cdot x+k_y\cdot y)}\, dxdy\,. \quad (4)$$

In this paper, the incident beam of Gaussian type is considered, which agrees with the general configuration in the QO feed instrument where the horns are designed to generate Gaussian-like beams that propagate in the routine guided by elliptical mirrors and FSSs (transparent or reflecting)[10-15]. In this case, the incident fields can be considered as band limited in the PWS (only propagating components are necessary to be considered in most cases). Therefore, the integration range of (2) and index range of (4) can be set to $k_x^2+k_y^2<k_0^2$.

On the other hand, if the reflected and transmitted fields are confined within the aperture of the FSS screen, then that can be considered as an infinite periodic structure for the incident beam. For that periodic structure with the period p_x and p_y, the $f^t_{\gamma\xi}(k_x,k_y,x,y)$ can be expressed as a summation of a set of Floquet harmonics:

$$f^t_{\gamma\xi}(k_x,k_y,x,y) = \sum_m \sum_n \alpha^{m,n}_{\gamma\xi}(k_x,k_y)\cdot \mathrm{e}^{-j\left[(k_x+\frac{2m\pi}{p_x})\cdot x+(k_y+\frac{2n\pi}{p_y})\cdot y\right]}. \quad (5)$$

Generally, for the FSS structure designed without grid-lobes in the pass band, only the basic mode (m=0, n=0) of Floquet harmonics is propagable. By taking other harmonics (evanescent wave components) into consideration, one can evaluate all the local-field effects caused by the FSS structure, which however will not propagate far off the structure before vanishing.

Given that only the basic mode of Floquet harmonics is considered, Eq. (2) can be simplified into:

$$\begin{pmatrix} E^t_x(x,y)|_{TA} \\ E^t_y(x,y)|_{TA} \end{pmatrix} = \iint_{\left(k_x^2+k_y^2<k_0\right)} \tilde{M}_a \cdot \begin{pmatrix} A^i_x(k_x,k_y) \\ A^i_y(k_x,k_y) \end{pmatrix} \frac{dk_x dk_y}{4\pi^2}, \quad (6a)$$

$$\tilde{M}_a(k_x,k_y,x,y) = \begin{pmatrix} \alpha_{xx}(k_x,k_y) & \alpha_{xy}(k_x,k_y) \\ \alpha_{yx}(k_x,k_y) & \alpha_{yy}(k_x,k_y) \end{pmatrix} \cdot e^{-j(k_x\cdot x+k_y\cdot y)}. \quad (6b)$$

Here and in the rest of this paper, the upper-script$^{(0,0)}$ for $\alpha_{\gamma\xi}(k_x,k_y)$ is omitted.

The four transmission coefficients, $\alpha_{\gamma\xi}(k_x,k_y)$, consist of the FSS transmission function in the PWS. Without the consideration of evanescent waves, the Eq. (6) is in form of Fourier transformation, and allows a more efficient field re-composition than that using Eq. (2).

The formulations for obtaining the transmitted H-fields on **TA** are similar to that for the E-fields, and are not listed here for brevity. Meanwhile, the discretization's in the PWS for implementing Eqs. (2), (4), and (6) will not be discussed in detail here, as can be referred to [6,8-9]. Generally, the sampling interval of k_x and k_y is related to the size of FSS screen to be modeled: as the size of FSS aperture rises, the sampling interval in the PWS have to decrease accordingly for avoiding space aligns [9].

In implementation, the FDTD-PWS hybrid approach in modeling the planar periodic structure under the beam illumination can be divided into two procedures:

1) Sweeping of PBC simulations to obtain $f^t_{\gamma\xi}(k_x,k_y,x,y)$ or $\alpha_{\gamma\xi}(k_x,k_y)$ at each frequency;
2) Incident beam decomposition using Eq. (4) and field re-composition using Eq. (2) or Eq. (6).

C. Wideband PBC for the FDTD-hybrid

The FDTD-PWS approach used in this paper is updated from that in [8, 9], by using the complex-field PBC [3] for the wideband computations. In the complex-field PBC method, the complex-fields are iteratively updated in the time domain, and the tangential component of the wave number $\boldsymbol{k}_\rho$ is fixed. As a result, the plane-wave incident direction angle θ varies with frequency f. The advantages of the complex-field PBC method over others such as the split-field method [2, 5], include improved computational efficiency especially in the large incident angle situation, being robust for arbitrary material properties, as well as simplicity in implementation.

From the PBC calculations, both the transmission coefficients $\alpha_{\gamma\xi}(k_x,k_y)$ and the field distribution $f^t_{\gamma\xi}(k_x,k_y,x,y)$ can be recorded at cared frequencies for the field re-composition purpose. In practical, it would be storage expensive to restore the $f^t_{\gamma\xi}(k_x,k_y,x,y)$ results for Eq. (2), especially when evaluations at a large number of frequencies are to be carried out. Meanwhile, the $\alpha_{\gamma\xi}(k_x,k_y)$ recording and the field re-composition by Eq. (6) can be much more efficient in storage and computation. However, the evanescent waves are dropped out in this manner, and the local-fields by the FSS structure cannot be observed in the re-composed field results. In the following sections, both the results by Eq. (2) and Eq. (6) will be presented and compared, for the analysis on the transmitted beam degradations through FSS.

III. VALIDATION OF METHOD

A. Validation of FDTD-PBC results

The FSS structure considered in this work is designed for the beam transmission from 215 GHz to 225 GHz, at the direction of (θ=30°, φ=180°). For the FDTD formulations, each periodic unit of this FSS can be

discretized into 30(x) × 30(y) × 50(z) Yee-cells. The calculated plane-wave coefficients by our in-house FDTD-PBC realization and one commercial software [18] are compared in Fig. 4.

As can be seen, the results match well with each other. This implies that the complex-field FDTD-PBC was implemented correctly for this study.

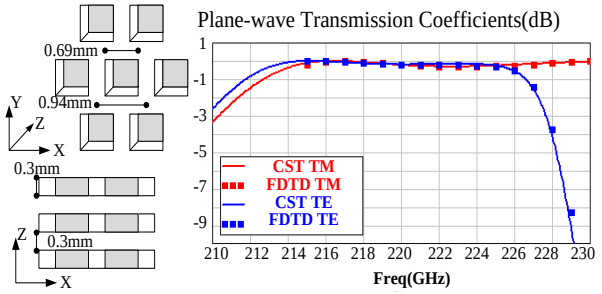

Fig. 4. Comparison of calculated plane-wave transmission coefficients (plane-wave incidence at θ=30°, φ=180°), dB.

In the PBC computation as well as in the field re-composition, the incident aperture **IA** and incident aperture **TA** are ten Yee-cells distant away from the FSS structure. That means the fields on an aperture that is very close to the FSS structure are investigated in this paper.

B. Validation of FDTD-PWS results

To validate the band FDTD-PWS hybrid method, we directly modeled the whole FSS screen by standard FDTD formulations to provide reference results, and the simulation in this way is denoted by "FDTD". Then on the transmitted aperture **TA**, field distributions calculated by the two methods due to normal beam incidence are compared in Fig. 7, and good agreements can be observed. We used Eq. (2) in the re-composition procedure of FDTD-PWS, so that the recomposed field distributions contain information of all the local-field effects by the FSS, and can be directly compared with that by FDTD. The incident beams considered in this set of simulations are of the Gaussian basic mode [10] with the waist radius ω_0 equaling 2λ, TM polarized. And in the Fig. 5, the beam transmission coefficient results are compared. For the FDTD-PWS method, results by Eq. (6) are presented, which agrees well with that by direct "FDTD" computations. That means, even on the aperture **TA** that is very close to the FSS structure, by using Eq. (6) for the field re-composition (considering only the propagable plane-wave components without evanescent ones) one can still investigate the beam transmission coefficient correctly and sufficiently.

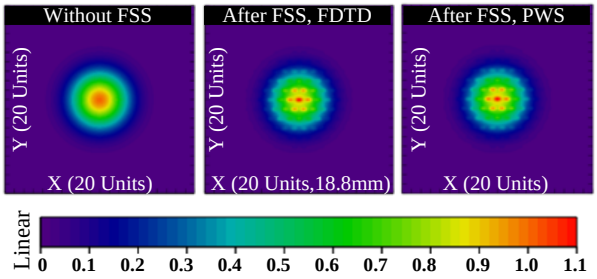

Fig. 5. Comparison of calculated transmission fields at 220 GHz on the transmitted aperture, by FDTD and FDTD-PWS (re-composition by Eq. (2)), normal beam incidence (ω_0 = 2λ, θ=0°, φ=180°), TM polarization, normalized by the maximum of reference free-space transmitted fields, linear.

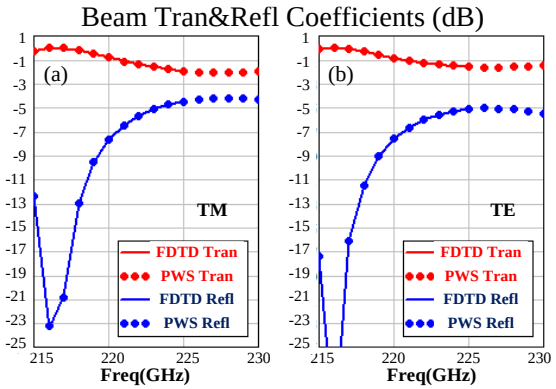

Fig. 6. Comparison of calculated beam transmission and reflection coefficients from 215 to 230 GHz, by the FDTD and band FDTD-PWS (Eq. 6), normal beam incidence (ω_0= 2λ, θ=0°, φ=180°), TE and TM polarization.

IV. SAMPLING IN K-DOMAIN AND COMPUTATION EFFICIENCY

In this section, the computation efficiency of the proposed FDTD-PWS method is discussed. First, an important issue is the sampling in the k_x-k_y domain. The discretized sampling in the k domain leads to periodic expansion in space domain. To model a planar FSS screen of aperture size L_ξ (ξ stands for x or y) without space alias, a sampling interval less than $k_0\lambda/L_\xi$ is necessary, leading to $2L_\xi/\lambda$ samplings in the k_ξ domain(-k_0~+k_0). After dropping evanescent compo-nents in the k_x-k_y domain ($k_x^2+k_y^2>k_0^2$), one requires PBC responses at $\pi L_xL_y/\lambda^2$ sampling positions for the PWS composition. By using an even smaller interval and a larger sampling number, field interference at aperture edges in the PWS composition (if exists) can be further reduced [9].

Actually, the main computation load of the FDTD-PWS is in the procedure of PBC simulations, which

requires calculations at a number $\pi L_x L_y/\lambda^2$ of k_x-k_y spectrum positions. Consider the same time duration in the FDTD computation, the CPU load for simulating a finite-sized FSS screen (consists of $Nx*Ny$ units, leading to aperture size of $L_x=N_xp$, $L_y=N_yp$) is $Nx*Ny*\mathbf{O}(C)$, as a reference. In PBC simulations for the FDTD-PWS hybrid, at one k_x-k_y sampling point, the CPU load is $4\mathbf{O}(C)$, due to requirements of complex field computation and TE/TM excitation. That leads to totally $4\pi NxNyp^2/\lambda^2$*O(C) for the PBC simulation procedure. Further, if symmetry exist in the FSS unit, the computation burden can be cut to $\pi NxNy*p^2/\lambda^2$*O(C). In an ideal case, the CPU computation load of PBC simulations is $\pi p^2/\lambda^2$ times to a direct FDTD simulation for the FSS screen with symmetric unit structure, and for the parameters in this paper, this factor is 1.64 (λ@230GHz, p = 0.94mm). Further, in practical, the k_x-k_y region may not need to be fully sampled in ($k_x^2+k_y^2<k_0^2$), as one doesn't require those results in case of large incident angles. Therefore sampling in the spectrum region $k_x^2+k_y^2<t^2k_0^2$ (t<1) should be sufficient. Here t = sin(θ_{max}), and θ_{max} is the maximum incident direction angle necessary to be considered in the PBC simulations[9].

Table 1: Comparison of CPU run times by FDTD-PWS and FDTD for FSS structures of different aperture sizes (On an Intel Core i7 desktop)

Array Size (in Units)	FDTD-PWS		FDTD
	PBC Runs	Re-composition by Eq. (2)	
28×28	12(h) 536 runs	24(s) per frequency	9(h)
36×36	24(h) 884 runs	64(s) per frequency	16(h)
46×46	32(h) 1424 runs	170(s) per frequency	—

Table 2: Comparison of memory costs by FDTD-PWS and FDTD for FSS structures of different aperture sizes

Array Size (in Units)	FDTD-PWS		FDTD
	PBC Runs	Re-composition by Eq. (2)	
28×28	52(MB)	227(MB)	2294(MB)
36×36	54(MB)	370(MB)	5076(MB)
46×46	56(MB)	599(MB)	—

In the above tables, the CPU run times and memory cost of the two methods are listed to be compared. The advance in computation efficiency of the FDTD-PWS hybrid is in the re-composition procedure. When treating varied beam incidence, such as the many illumination cases considered in the next chapter, the FDTD-PWS requires only minutes to harvest results, meanwhile the FDTD need repeated direct computations costing hours. On the other hand, as the FDTD-PWS hybrid performs computation within a unit cell, the reduction of memory cost over FDTD for modeling the FSS screen should also be remarked.

V. DISCUSSIONS ON THE BEAM DEGRADATION

Here, the cases of oblique beam incidence are considered, where the incident beams are illuminating at the direction of (θ=30°, φ=180°), TE and TM polarized separately. The transmitted field distributions on **TA** calculated by both FDTD and FDTD-PWS (using Eq. (2)), are presented in Fig. 7, while the fields on **TA** but through free-space are also draw as references. Clearly those results of transmitted fields through FSS by the two methods agree well. It is worth noting that, to obtain results in Fig. 7 by the "FDTD" solution, repeating computations have to be performed. On the contrary, in the FDTD-PWS hybrid method, only the field re-composition procedure is required based on the restored PBC calculate results. As a result, the comparison between the computation times by two approaches for this problem, can be hours (FDTD) to minutes or even seconds (FDTD-PWS).

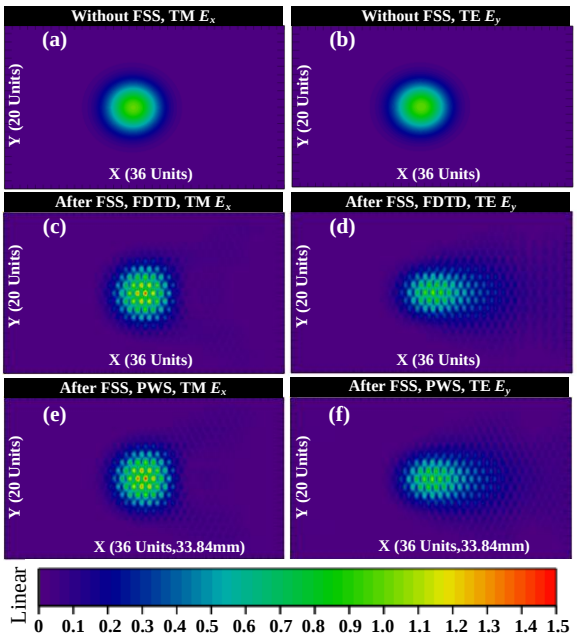

Fig. 7. Comparison of calculated transmission fields at 220 GHz on the transmitted aperture, by FDTD and FDTD-PWS (re-composition by Eq. (2)), oblique beam incidence ($\omega_0=2\lambda$, θ=30°, φ=180°), TE and TM polarization, normalized by the maximum of reference free-space transmitted fields, linear.

On the other hand, it is evident that, in the transmitted field distributions, beam distortions can be observed in

both the cases of TE and TM incidence. Also the transmitted beams show tangential shifts comparing to the referencing free-space transmitted beam. And the distortions in the TE transmitted beam are more severe than that in the TM transmitted beam. Meanwhile, the transmitted field distributions calculated by using Eq. (6) (without all the evanescent waves) are presented in Fig. 8. It is clear to readers that, the same distortion patterns in the transmitted field distributions in either the TE or TM incident case, are shared in the results by Eq. (2) and by Eq. (6). That implies, the reason for the transmitted beam distortions, should be blamed to the $\alpha_{\gamma\zeta}(k_x,k_y)$ distributions, which define the FSS response to each incident plane-waves as in Eq. (6).

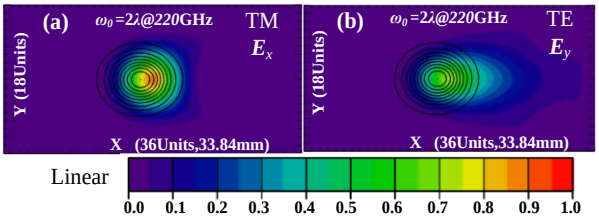

Fig. 8. Calculated transmission fields at 220 GHz on the transmitted aperture, by FDTD-PWS (using Eq. (6)), oblique beam incidence (ω_0 = 2λ, θ=30º, φ=180º), TE and TM polarization, normalized by the maximum of reference free-space transmitted fields (black lines contoured), Linear.

It would be interesting and intuitive to investigate the beam distortion effects by the FSS via $\alpha_{xx}(k_x,k_y)$ and $\alpha_{yy}(k_x,k_y)$ in the PWS, the magnitude distributions of which are contoured in Fig. 10 at different frequencies. When the beam incident direction is in the XOZ plane (φ=180º), the $\alpha_{xx}(k_x,k_y)$ plays a significant role for transmission of the TM polarized beam, while the $\alpha_{yy}(k_x,k_y)$ is vital for transmission of the TE one. In Fig. 10, spectrum regions covered by the incident spectrum $A^i_\xi(k_x,k_y)$ with the edge level of -20dB are closely curved, in cases of the waist radius ω_0 of incident Gaussian beam equaling 2λ and 4λ. Apparently when ω_0 increases, the corresponding spectrum coverage area decreases. However, in the practical design of QO instruments, more spaces are required by designers for placing corresponding elliptical reflectors [10], if a larger waist radius ω_0 of the propagating beam is to be realized.

It is evident that, when beams of ω_0 = 2λ are illuminating at 220 GHz, distributions of neither $\alpha_{xx}(k_x,k_y)$ nor $\alpha_{yy}(k_x,k_y)$ are flat in magnitude within the spectrum region covered by the incident beam (Fig. 10 (c) or (d)). Meanwhile, transmitted beam distortions occur. It is also interesting, to observe the relationship between the $\alpha_{xx}(k_x,k_y)$ distribution pattern and TM transmitted beam distortions, and that between $\alpha_{yy}(k_x,k_y)$ and the severely distorted TE transmitted beam (Fig. 8 and Fig. 10). The non-flatness patterns in $\alpha_{\xi\xi}(k_x,k_y)$ reveal themselves accordingly in the transmitted field distributions due to the corresponding polarized beam incidence. On the other hand, if the incident beams of ω_0 = 4λ are illuminating, the incident spectrum region are smaller in size. As a result, the area of non-flatness in $\alpha_{xx}(k_x,k_y)$ and $\alpha_{yy}(k_x,k_y)$ distributions are greatly reduced in percentage. The corresponding transmitted fields distributions by Eq. (6) are presented in Fig. 9. It can be seen that, the TM transmitted fields is nearly clean of distortions. Meanwhile, the TE transmitted fields still suffer notable distortions, as in the $\alpha_{yy}(k_x,k_y)$ distribution "cliff" exists in the edge area of spectrum region covered by the incident Gaussian beam (ω_0 = 4λ).

It is also intuitive to observe the transmitted beam propagation off the FSS structure in the vertical cut, the results of which at 220 GHz are presented in Fig. 11. Those results are by Eq. (6) and PWS propagation equations. At another view, the transmitted beam distortions can be observed, especially those in the TE transmitted beams due to the $\alpha_{yy}(k_x,k_y)$ magnitude "cliff" as in Fig. 10 (d).

Another interesting trend concluded from Fig. 10 is that, the area of flat $\alpha_{\xi\xi}(k_x,k_y)$ distributions are shrinking in size, as the frequency rise from 217 GHz to 225 GHz. That trend can also be observed in the beam transmission coefficient results presented in Fig. 12, that the curves of results is heading downside in the specific frequency region. And, as the incident beam waist width ω_0 in the spatial domain increases, the corresponding spectrum coverage area decreases. As a result, beam transmission coefficients are more close to the plane-wave ones, while beam distortions can be relieved.

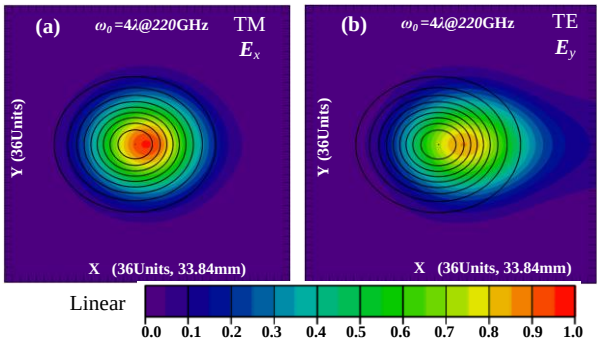

Fig. 9. Calculated transmitted E-fields at 220 GHz on the transmitted aperture, by FDTD-PWS (using Eq. (6)), oblique beam incidence (ω_0 = 4λ, θ=30º, φ=180º), TE and TM polarization, normalized by the maximum of free-space transmitted fields (black lines contoured), linear.

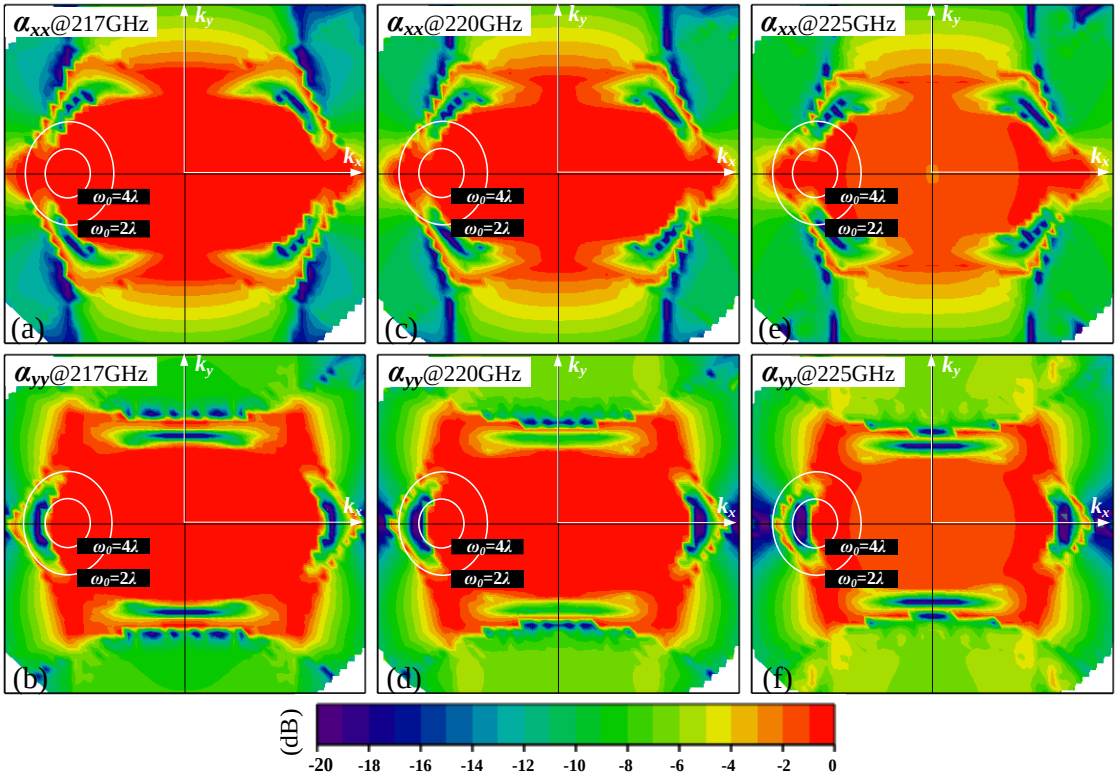

Fig. 10. Comparison of calculated plane-wave transmission coefficients of $\alpha_{xx}(k_x,k_y)$(first row) and $\alpha_{yy}(k_x,k_y)$ (second row), at 217 GHz (first column), 220 GHz (second column), and 225 GHz (third column), dB; spectrum regions (with -20 dB edge level) covered by the beam incidence of different $\omega_0(\theta=30^o, \varphi=180^o)$ are closely curved.

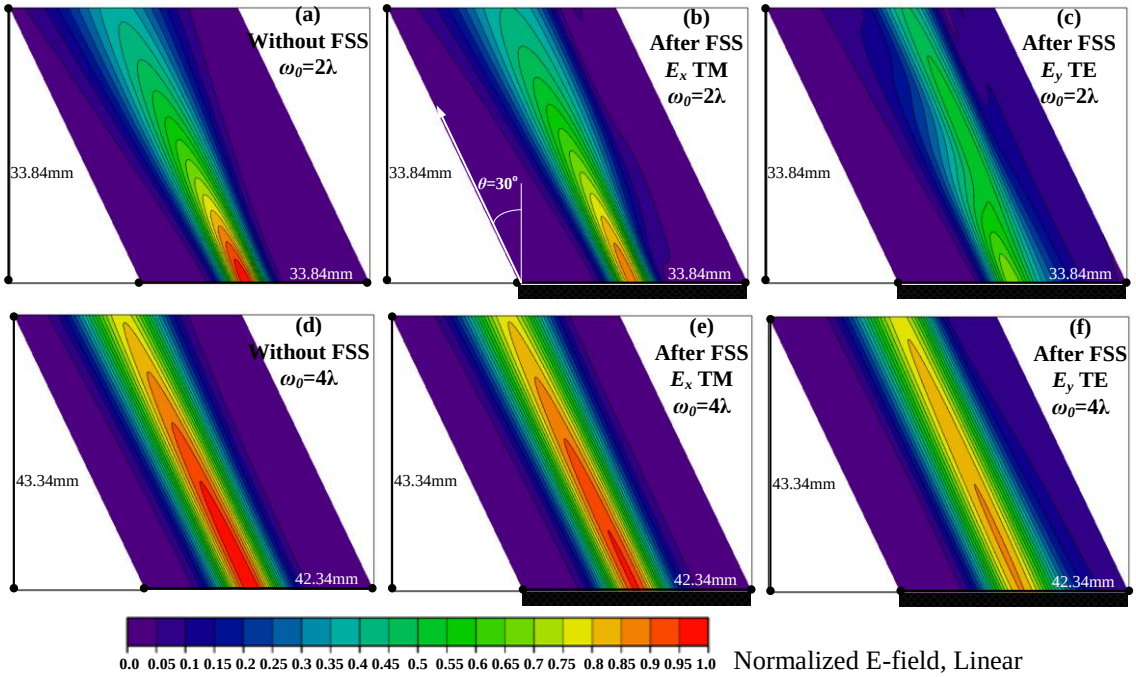

Fig. 11. Transmitted beam distributions in the vertical cut, oblique beam incidence of different $\omega_0(\theta=30^o, \varphi=180^o)$, TE or TM polarized, @ 220 GHz. The results are obtained by Eq. (6), in magnitude, linear, normalized by maximum of free-space transmitted beam.

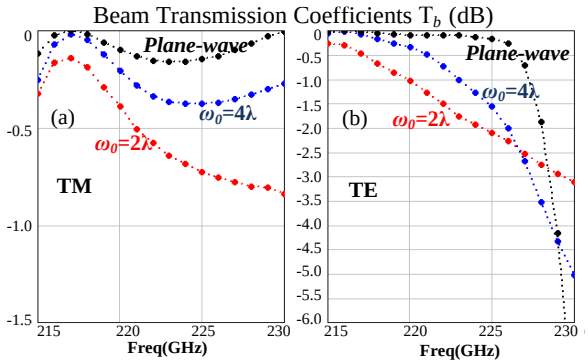

Fig. 12. Comparison of calculated beam and plane-wave transmission coefficients, oblique beam incidence (θ=30°, φ=180°), TM and TE polarization, dB.

It can be concluded that, the observed beam distortion is due to the non-flatness of the transmission coefficients distribution in spectrum region covered by the beam incidence. And, the investigation on $\alpha_{\xi\xi'}(k_x,k_y)$ in the PWS provides an intuitive perspective for evaluating and diagnosing the beam propagation through an FSS.

At last, another set of the calculated T_b results are presented in Fig. 13, which are under beam incidence towards different directions. The varying trends of T_b versus beam incident direction can be clearly observed. These results contain information cared by QO designers in the practical design and optimization process, and can be efficiently obtained by the band FDTD-PWS hybrid method.

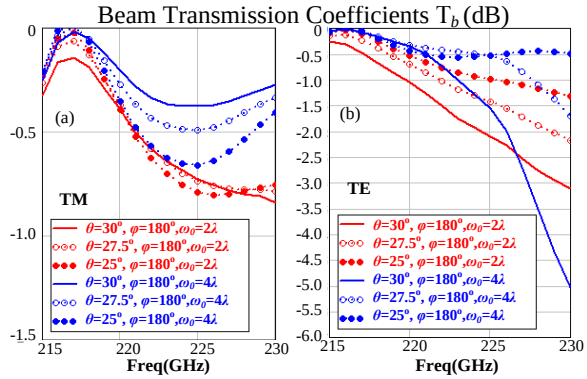

Fig. 13. Comparison of the calculated beam transmission coefficients at different beam incident angles, with the waist radius ω_0 = 2λ or 4λ; the beam transmission coefficients are obtained by the band FDTD-PWS; TM and TE polarization, dB.

VI. CONCLUSION

With implementation of the wideband complex-field PBC technique for modeling the FSS unit, we updated and completed the FDTD-PWS hybrid method. The proposed method takes advantage of the FDTD method in the wideband computation ability, while the PBC simulation results can be re-used in the rapid re-composition for fields due to variable beam incidence. Consequently, it meets the need of efficient beam transmission evaluation through FSS within the frequency band of interest. The solution has been validated by results of standard FDTD formulations in directly modeling the whole finite-sized FSS screen.

The degradations of the transmitted beams through a dual-polarized FSS design were studied, and that of TE polarized beams are more severe than that of TM polarized beams. Actually, it can be concluded that the observed beam distortion is highly related to the non-flatness in the magnitude distribution of plane-wave transmission coefficients, in the spectrum region covered by the beam incidence. It is demonstrated in this work that, the beam transmission performance of an FSS can be evaluated directly in the PWS, even on an aperture very close to the FSS structure. And such a spectrum analysis manner provides an intuitive perspective for the beam propagation diagnostic through periodical structures, especially for the practical design and optimization of full-polarized millimeter Quasi-Optical (QO) instruments.

ACKNOWLEDGMENT

This work is supported by the National Basic Research Program of China (973 Program) under Grant 2012CB315601.

REFERENCES

[1] R. Mittra, C. Chan, and T. Cwik, "Techniques for analyzing frequency selective surfaces: A review," *IEEE Proceedings*, vol. 76, pp. 1593-1615, 1988.

[2] J. Roden, S. Gedney, M. Kesler, J. Maloney, and P. Harms, "Time domain analysis of periodic structures at oblique incident: Orthogonal and non-orthogonal FDTD implementations," *IEEE Trans. Microwave theory Tech.*, vol. 46, no. 4, pp. 420-427, 1998.

[3] F. Yang, J. Chen, R. Qiang, and A. Elsherbeni, "A simple and efficient FDTD/PBC algorithm for scattering analysis of periodic structures," *Radio Science*, vol. 42, RS4004, 2007.

[4] K. ElMahgoub, F. Yang, A. Z. Elsherbeni, V. Demir, and J. Chen, "FDTD analysis of periodic structures with arbitrary skewed grid," *IEEE Trans. Antennas Propagat.*, vol. 58, no. 8, pp. 2649-2658, 2010.

[5] M. Bai, B. Liang, and H. Ma, "An efficient FDTD algorithm to analyze skewed periodic structures impinged by obliquely incident wave," *Journal of the Applied Computational Electromagnetic Society*, vol. 30, no. 10, pp. 1068-1073, 2015.

[6] M. Pasian, M. Bozzi, and L. Perregrini, "Accurate modeling of dichroic mirrors in beam-waveguide

antennas," *IEEE Trans. Antennas Propagat.*, vol. 61, no. 4, pp. 1931-1938, 2013.

[7] V. Prakash, N. T. Huang, and R. Mittra, "Accurate analysis of interaction between microwave antennas and frequency selective surface (FSS) radomes," *ICAP 2003*, vol. 1, pp. 401-404, March 31-April 3, 2003.

[8] M. Jin, M. Bai, N. Ou, and J. Miao, "The plane-wave approach for beam transmission through planar FSS structures," *ICMMT 2012, IEEE International*, pp. 128-131, May 2012.

[9] M. Bai, M. Jin, N. Ou, and J. Miao, "On scattering from an array of absorptive material coated cones by the PWS approach," *IEEE Trans. Antennas Propagat.*, vol. 61, no. 6, pp. 3216-3224, 2013.

[10] P. Goldsmith, *Quasi-optical Systems: Gaussian Beam Quasi-optical Propagation and Applications*. Piscataway, NJ, IEEE Press, 1998.

[11] R. Martin and D. Martin, "Quasi-optical antennas for radiometric remote sensing," *Electronics and Commnications Engineering Journal*, vol. 8, no. 1, pp. 37-48, 1996.

[12] L. Costes, C. Bushell, M. Buckley, et al., "Microwave humidity sounder (MHS) antenna," *Proc. SPIE*, 3870, pp. 412-426, 1999.

[13] R. Jorgensen, G. Padovan, P. de Maagt, D. Lamarre, and L. Costes, "A 5-frequency mili-meter wave antenna for a spaceborne limb sounding instrument," *IEEE Trans. Antennas Propagat.*, vol. 49, no. 5, 2001.

[14] S.-W. Zhang, J. Li, Z.-Z. Wang, et al., "Design of the second generation microwave humidity sounder (MWHS-II) for Chinese meteorological satellite FY-3," *Proc. IGARSS'12*, Munich, pp. 4672-4675, 2012.

[15] M. Candotti, A. Baryshev, and N. Trappe, "Quasi-optical assessment of the ALMA band 9 front-end," *Infrared Physics & Technology*, vol. 52, no. 5, pp. 174-179, 2009.

[16] R. Qiang, J. Chen, and F. Yang, "Finite difference time domain modeling of finite-sized electro-magnetic source over periodic structure via a plane wave spectral expansion approach," *Radio Science*, vol. 45, RS5003, 2010.

[17] R. Qiang, J. Chen, F. Capolino, and D. R. Jackson, "ASM-FDTD: a technique for calculating the field of a finite source in the presence of an infinite periodic artificial material," *Microwave and Wireless Components Letters, IEEE*, vol. 17, no. 4, pp. 271-273, 2007.

[18] https://www.cst.com/Products/CSTMWS

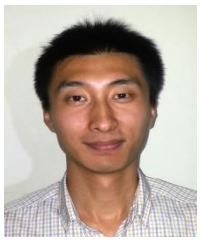

Ming Jin received his B.Sc. and Ph.D. degrees from Beihang University (BUAA), Beijing, China, in 2007 and 2013, respectively. From 2007 to 2013, he has been a Research Assistant in the Microwave Engineering Laboratory, Beihang University. From Dec. 2010 to Mar. 2011, he was a Visiting Scholar at Arizona State University. From 2013 to 2015, he was with the Science and Technology on Electromagnetic Scattering Laboratory. He is now with the State Key Laboratory of Remote Sensing Science, Institute of Remote Sensing and Digital Earth, Chinese Academy of Sciences. His research interests include, computational electromagnetic and microwave imaging.

Ming Bai received his B.Sc. and Ph.D. degrees from Physics Department of the University of Science and Technology of China (USTC) in 1996 and 2002, respectively. From 2002 to 2006, he worked as a Postdoctoral Researcher in the Laboratory of Nano-technology (LFSP), Spanish National Research Council (CSIC). He joined Beihang University (BUAA) China, in 2006. Currently he worked as a Professor in Microwave Engineering Lab., Beihang University. His research interests include computational electromagnetic and microwave imaging.